Effect of the particle surface charge density on the colloidal aggregation mechanism

A. Fernández-Barbero, M. Cabrerizo-Vílchez, R. Martínez-García, and R. Hidalgo-Álvarez
Grupo de Física de Fluidos y Biocoloides, Departamento de Física Aplicada, Universidad de Granada, 18071 Granada, Spain
(Received 2 August 1995)

We have studied the influence of the surface charge density of polymer colloids on the aggregation processes induced at a high salt concentration. In this way, the effect of the residual interaction between the particles on the aggregation mechanism was studied. The time dependence of the detailed cluster-size distribution and the time-independent scaling distribution were obtained by single particle light scattering. We found a change in the aggregation mechanism, expressed as a variation of the μ exponent value, when the surface charge was modified.

PACS number(s): 64.60.Cn, 05.40.+j, 82.70.Dd

I. INTRODUCTION

In the last decade, models have been developed describing the structure which results from the union of subunits. The aggregation of colloidal particles is a good model for describing this phenomenon, central to many physical [1], chemical [2], and biological [3] processes. Determining the detailed cluster-size distribution is important since many of the properties of a colloid depend on that distribution, and by now, the number of theoretical predictions and computer simulations on the form and time dependence of the cluster-size distribution far exceed the number of experimental results. Both theory and experiments have shown a universal behavior, independent of the colloid, when the aggregation of clusters is diffusion limited (DLCA) or reaction limited (RLCA) [4–11]. DLCA occurs when every collision between diffusing clusters results in the formation of a bond. In this regime, the rate of aggregation is limited by the time it takes clusters to diffuse towards one another. RLCA occurs when only a small fraction of collisions between clusters leads to the formation of bigger clusters. In this case, the rate of aggregation depends not only on the diffusion of the clusters, but also on the time it takes clusters to form a bond. The two most prominent features of the universal behavior are reaction kinetics and cluster morphology. The former is described using Smoluchowski's coagulation equation [12] and the latter by considering clusters as fractal structures [13,14].

The aggregation mechanism depends on the interaction between clusters. The latter may be modified by adding a salt to a stable colloid. This reduces the electrostatic interaction at large distances, but keeps a big value for the short range residual interaction. In fact, to ensure DLCA conditions, hydrochloric acid (HCl) is usually added to a system of negatively charged particles to eliminate their surface charge density [10]. The basic question we will address is how does this residual interaction affect the aggregation kinetics. When aggregation is induced at a high salt concentration, the repulsive potential is screened and highly localized around the particles. Under these conditions, an irreversible fast process takes place, primarily due to the Brownian motion of the colloidal particles. In order to control the residual potential, it is necessary to act directly on the particle surface charge density. This may be performed by modifying the degree of ionization of the surface ionic groups by changing the pH of the solvent.

In this paper we address the following question: how does the particle surface charge density affect the aggregation kinetics in processes induced at high salt concentration? In other words, how does the aggregation mechanism depend on the residual interaction between the particles? The detailed cluster-size distribution of aggregating colloids of polystyrene microspheres, was measured by single particle light scattering [15–22]. We carried out a series of measurements for different surface charge densities. Dynamic scaling was found in all the cases studied; i.e., cluster distribution can be expressed in the factorized form

$$N_n(t) \sim s^{-2} \Phi(n/s), \tag{1}$$

where N_n is the concentration of clusters made up by n monomers, $s(t)$ a function of the number-average mean cluster size, and $\Phi(x)$ a time-independent scaling distribution, which characterizes the aggregation mechanism. This scaling form has also been observed in other experimental systems [8,23,24] and by numerical simulations [25]. At low surface charge densities we find that $\Phi(x)$ is bell shaped. When the surface charge is increased, the maximum shifts to lower x values. In contrast, at the highest charge density, $\Phi(x)$ decreases monotonically. In every case we found $s(t) \sim t$. Parameters λ and μ of the Van Dongen and Ernst classification for homogeneous kernels [26] were determined from the behavior of $s(t)$ and $\Phi(x)$ and features of the microscopic mechanisms which govern the aggregation were deduced.

The outline of this paper is as follows: Sec. II is a theoretical background; the experimental system, technique, and experimental details are described in Sec. III; results are reported and discussed in Sec. IV; the conclusions are in Sec. V.

II. KINETICS OF GROWTH

We interpret our results using the Smoluchowski rate equation which provides a useful mean field approach to the kinetics and a framework to classify a wide variety of growth processes. This classification helps to distinguish between DLCA and RLCA and to clarify the difference between aggregation and gelation processes, frequently observed in col-

loidal systems. In general, a colloidal aggregation process may be described by the following reaction scheme:

$$(i\text{-mer})+(j\text{-mer})\xrightarrow{k_{ij}}(i+j)\text{-mer}, \tag{2}$$

where i-mer denotes a cluster of i subunits and $k_{ij}=k_{ji}\geqslant 0$ is the concentration-independent coefficient or kernel of the irreversible reaction. This kernel parametrizes the rate of such a reaction, giving the probability of an i-mer reacting with a j-mer. Kernels contain the physical information on the aggregation process and, in general, depend on the size of the reacting clusters. A kernel is a configurational and orientational average of the reaction rate between two colliding clusters. For diluted suspensions, only collisions between two clusters need be considered, since the probability of a three-cluster collision is negligible.

Coagulation equation. Smoluchowski's equation [12] expresses the time evolution of the cluster-size distribution, $N_n(t)$, in terms of the reactions kernels k_{ij}

$$\frac{dN_n}{dt}=\frac{1}{2}\sum_{i+j=n}k_{ij}N_iN_j-N_n\sum_{i=1}^{\infty}k_{in}N_i. \tag{3}$$

This equation takes into account all the pairs of collisions which may generate or deplete a given cluster size. The first term accounts for the creation of n-mers through binary collisions of i-mers and $(n-i)$-mers. The second one represents the depletion of n-mers due to binary collisions with other clusters. The structure of this equation is simple, although, it is difficult to know the form of the reaction kernel for a given system. Smoluchowski's equation is analytically solvable only for a few kernels; for example, constant kernel ($k_{ij}=k_{11}$), sum kernel ($k_{ij}\sim i+j$), product kernel ($k_{ij}\sim ij$), and linear combinations thereof. For monomeric initial conditions and constant kernel, the solution is given by [27]

$$N_n(E)=N_0\,\frac{E^{n-1}}{(1+E)^{n+1}}, \tag{4}$$

where N_0 is the initial monomer concentration and $E\equiv t/t_{\text{agg}}\equiv tN_0k_{11}/2$.

Homogeneous kernels. Most coagulation kernels used in the literature are homogeneous functions of i and j, at least for large i and j [28–30]. Van Dongen and Ernst [26] introduced a classification scheme for homogeneous kernels, based on the relative probabilities of large clusters sticking to large clusters, and small clusters sticking to large clusters. If the small-large interactions dominate, then large variations in the cluster mass are discouraged, and the size distributions will tend to be tightly bunched together, like a bell-shaped curve. If large-large interactions dominate, the small clusters tend to be left behind in the scramble and the result is a monotonically decreasing size distribution. In this theory it is assumed that, in the scaling limit, i.e., long times and large clusters, the cluster-size distribution has the form [26,31,32]

$$N_n(t)\sim s^{-\theta}\Phi(n/s), \tag{5}$$

where θ is a kinetic exponent, $s(t)$ is related to the average cluster size, and $\Phi(x)$ is the time-independent scaling function. A direct consequence of mass conservation is $\theta=2$.

Dependence of homogeneous kernels on i and j at large i and/or j, may be characterized by two exponents defined as follows:

$$k_{ai,aj}\sim a^{\lambda}k_{i,j}\quad(\lambda\leqslant 2), \tag{6}$$

$$k_{ij}\sim i^{\mu}j^{\nu}\quad(\nu\leqslant 1),\quad i\ll j,\ \lambda=\mu+\nu. \tag{7}$$

Kernels with either, $\lambda>2$ or $\nu>1$ are unphysical, since the reactivity cannot increase faster than the cluster mass. No restrictions are imposed on μ.

The homogeneity parameter λ describes the tendency of a big cluster to join up with another big cluster. For $\lambda>1$ the rate of aggregation becomes so fast that an infinite-size cluster forms in finite time and a gelation process occurs. Kernels with $\lambda\leqslant 1$ give nongelling behavior, i.e., an infinite cluster is formed at infinite time. Thus, the magnitude of λ allows us to distinguish between gelling and nongelling systems. λ takes the value 0 in DLCA, and 1 in the case of RLCA [53].

The exponent μ establishes the rate at which big clusters bind to small clusters and its sign determines the shape of the size distribution. For $\mu<0$ the big cluster-small cluster unions are favored and large clusters gobble up small ones resulting in a bell-shaped size distribution. Kernels with a negative μ appear to be a good description for DLCA. When $\mu>0$ the large-large interaction dominates and the size distributions resulting from such kernels tend to be polydisperse since small clusters may still exist even in the presence of large ones. Thus, distribution decays monotonically with increasing n.

Both $s(t)$ and $\Phi(x)$ in (5) contain the exponents λ and μ of the kernels [26,33]. For the function $s(t)$

$$s(t)\sim\begin{cases}t^{1/1-\lambda} & \lambda<1\\ \exp(\alpha t) & \lambda=1,\end{cases} \tag{8}$$

where α is a constant. This function is related to some ratios of moments of the cluster-size distribution. It is directly proportional to the weight-average mean cluster size $\langle n_W\rangle\equiv M_2/M_1$, where $M_i=\Sigma n^iN_n$, $s(t)$ is also related to the number-average mean cluster size $\langle n_n\rangle\equiv M_1/M_0$. The relationship between $s(t)$ and $\langle n_n\rangle$ depends on the sign of μ. For kernels with $\lambda<1$ [33,34]

$$s(t)\sim\begin{cases}\langle n_n\rangle & \mu<0\\ \langle n_n\rangle^{1/(2-\tau)} & \tau<1+\lambda,\ \mu=0\\ \langle n_n\rangle^{1/(1-\lambda)} & \mu>0\end{cases} \tag{9}$$

The analytical form of $\Phi(x)$ is known for large and small x [26,33]

$$\Phi(x\gg 1)\sim x^{-\lambda}\exp(-\beta x), \tag{10}$$

$$\Phi(x\ll 1)\sim\begin{cases}\exp(-x^{-|\mu|}) & \mu<0\\ x^{-\tau} & \tau<\lambda+1,\ \mu=0\\ x^{-(1+\lambda)} & \mu>0.\end{cases} \tag{11}$$

For large x, $\Phi(x)$ decreases and is related only to the exponent λ, where β is a fitting parameter. For small x, $\Phi(x)$ depends on the sign of μ. Therefore, when $\mu<0$, $\Phi(x\ll 1)$ increases with x, whilst for $\mu\geqslant 0$, $\Phi(x\ll 1)$ decays monotonically. Thus, the shape of the function $\Phi(x)$ depends critically

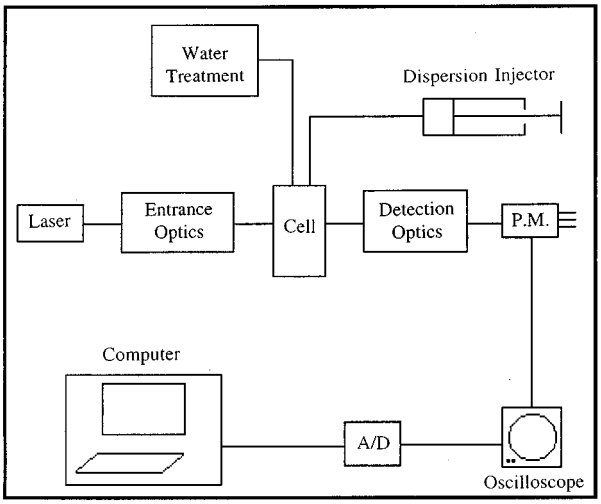

FIG. 1. Block diagram of the experimental system.

on the sign of μ. For kernels with $\mu<0$, $\Phi(x)$ is a bell-shaped function, whilst for $\mu\geqslant 0$, it decreases monotonically. If $|\mu|\to 0$, an intermediate x range exists, $x_0 \ll x \ll 1$, where kernels with $\mu>0$ and $\mu<0$ show typical $\mu=0$ behavior, with crossover to, respectively, $\mu>0$ and $\mu<0$ behavior at $x\sim x_0$, x_0 depends on μ as $x_0=\exp(-1/|\mu|)$ [26].

The above formulas (8) and (11) imply the following predictions for the long time behavior of the cluster-size distribution $N_n(t)$ (5). Thus, when $\lambda<1$

$$\begin{cases} \dfrac{N_n(t)}{N_1(t)} \to \infty & \mu<0 \\ N_n(t)\sim t^{-w} n^{-\tau} & w>1,\ \tau<1+\lambda,\ \mu=0, \\ N_n(t)\sim t^{-1} n^{-(1+\lambda)} & \mu>0 \end{cases} \quad (12)$$

III. MATERIAL AND METHODS

A. The single particle light scattering instrument

A single particle optical sizer was built in our laboratory [35,50] based on the device of Pelssers, Stuart, and Fleer [17]. In this technique, single clusters, insulated by the hydrodynamic focusing of a colloidal dispersion, are forced to flow across a focused laser beam. A measurement of the cluster-size distribution is performed by analyzing the light intensity scattered by the single clusters at a low angle, where intensity is monotonically related to the square cluster's volume: $I_n(\theta)/I_1(\theta)=n^2\sim V^2$. Under this condition, the scattered light intensity is high enough to detect particles accurately and the strong sensibility of the scattered light intensity on the particle's volume, makes it possible for a high resolution to be achieved. For longer angles the intensity is lower and data interpretation become difficult due to the intensity oscillations appearing when the particle size changes [36].

Figure 1 shows a block diagram of the instrument. Basically, it is a flow ultramicroscope in which pulses of light from the single particles are detected. Light from a laser goes through an input optical system in order to create a homogeneously illuminated zone at the center of the flow cell, where the cluster separation is performed. Single particles cross this illuminated zone, scattering pulses of light. Detection optics select only the light scattered at a low angle and focuses it onto a photomultiplier which supplies a proportional electrical current. This signal is converted into voltage and digitalized. A computer controls the analog to a digital converter board, and recognizes, classifies and counts the pulses by running an algorithm on line. Size distribution is obtained by representing the counts versus the pulse intensity.

An important requirement is that every particle receive the same incident intensity to ensure that the scattered intensity be related only to the particle size. Furthermore, a small detection volume is essential to guarantee the single particle detection. A focus with an elliptical cross section satisfies both requirements. Light from a 10 mW TEM_{00} Helium-Neon laser model GLG5410 (NEC, Japan) passes through a spatial filter. The elliptical focus is performed by passing the laser beam through two cylindrical lenses and focusing it with a microscope objective (Entrance Optics). In the focusing cell a colloidal dispersion is injected into a fast flowing water stream thereby obtaining a narrow particle stream. This crosses the laser beam creating a small scattering volume. There should not be more than one particle in the scattered volume. That is why the volume must be small and the particle concentration low. The maximum particle concentration allowed for an optimum single particle detection is of the order of 10^7 cm^{-3}.

Dust particles reduce instrument resolution and modify the size distribution. Therefore the cell must be kept free from contaminants. Fresh twice-distilled water (using Millipore equipment) was distilled again on line to avoid air bubbles. This water was pumped into a 7 nm tangential filter (Carbosep. Rhône Poulenc, France) by a gear pump (Tuthill Corp. U.S.A.). This filter prevents solid contamination and provides a continuous flux without pulse effects. The inner flux was controlled by two valves located between the tangential filter and the cell. Finally, dust correction was carried out by subtracting the counts measured with the supernatant only, from the size distribution.

Pulses of light scattered by the single clusters are collected by the detection optics. This is formed by a beam stop and a diaphragm, which allows only the light scattered between 2.7° and 3.2° to pass. This light was collected by a microscope objective (Melles Griot, 21 mm work distance) focused on the scattered volume. The selected light was focused on a diaphragm pinhole which blocks reflections from the cell windows and allows only the light scattered by the particles to pass. Then, a photomultiplier (R2228, Hamamatsu, Japan) detects the scattered light as current Gaussian pulses, which are transformed into voltage and amplified. The new signal was fed into an analog to digital converter board (DT-2830, Data Translation), working at a sampling frequency of 250 kHz. This sampling frequency is high enough to follow the pulses accurately. At the same time, a computer program, running on line, detects and classifies the pulses following two alternative algorithms: the first one detects the maximum of the Gaussian pulse, whereas the second one integrates the pulse, with the value of this integral being proportional to the pulse height. The height of the pulse, as well as its area, are related to the intensity of the scattered light and therefore, to the particle

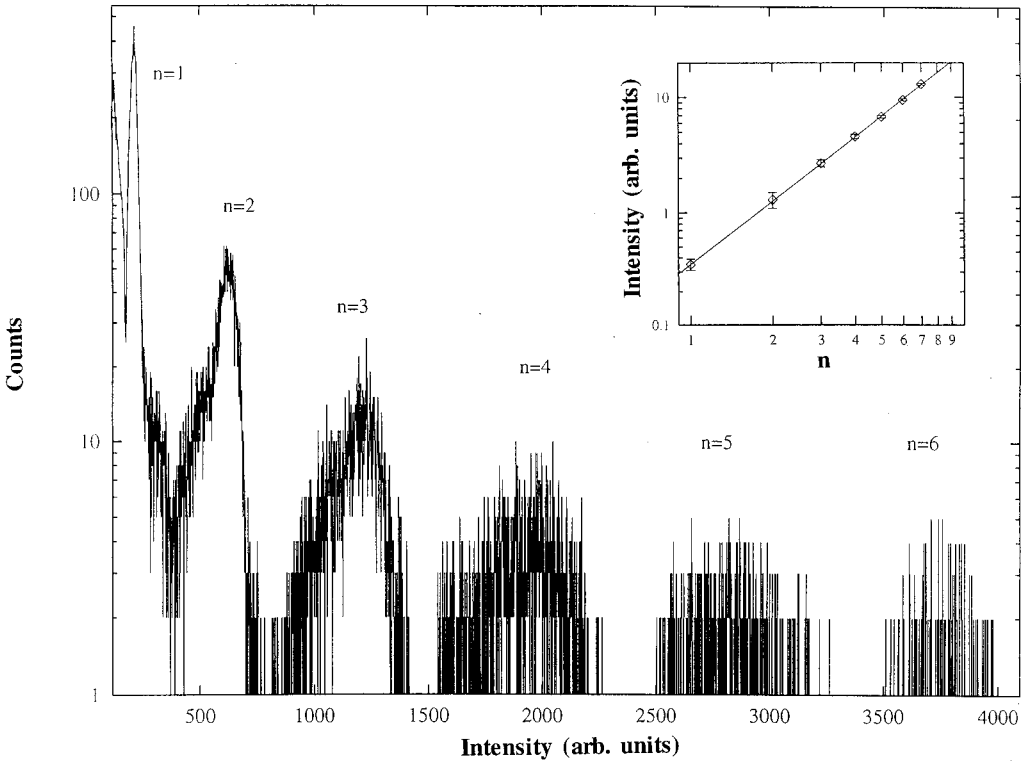

FIG. 2. Typical frequency histogram of an aggregating sample. Clusters from monomers up to hexamers are shown. The last channel (not shown) records the total number of off-scale pulses, enabling M_0 to be determined. The variation of the scattered light intensity with aggregation number (cluster's volume) is plotted at the upper right hand corner.

size. A frequency histogram can be obtained by plotting counts versus pulse intensity (~particle size) and thus, a simple particle counting procedure provides the size distribution. These new data acquisition procedures are an important modification with respect to the device of Pelssers, Stuart, and Fleer. No multichannel analyzer is necessary and thus, the particles can be detected without any special treatment of the photomultiplier output signal.

B. Determining cluster-size distributions

Figure 2 shows a frequency histogram of an aggregating latex dispersion (Sekisui-N1A19E). The peaks correspond to different cluster sizes from singlets to hexamers. Bigger clusters may be detected but it is difficult to distinguish between them. This instrument allows the detailed cluster-size distribution to be measured up to $n=6$ or 7, without applying numerical peak separation methods. The relationship $I \sim V^{(1.85\pm0.04)}$, between scattered light intensity and the volume of the clusters was found, which is close to Rayleigh's prediction $I \sim V^2$. The cluster-size distribution is determined by integrating the peaks appearing in the histograms, and the time evolution is obtained by analyzing a consecutive series of the latter. The statistical counting error $N_n^{1/2}$ was considered, being a criterion to set the time of measurement. The zero moment of the cluster-size distribution $M_0=\Sigma N_n$ is measured by adding the total number of counts in a histogram, including off-scale pulses. In this calculation every cluster must be counted, though they need not be separated according to their size. It allows the number-average mean cluster size $\langle n_n \rangle = N_0/M_0(t)$ to be calculated. This is related to $s(t)$ and is needed together with the distribution $N_n(t)$, to determine the scaling function $\Phi(x)$.

Hydrodynamic forces acting on aggregates could break them up under certain conditions. These forces are related to the stream velocity in the longitudinal and transversal directions with respect to the particle movement. Extensional and shear forces appear, respectively. These forces are also proportional to the extensional and shear rates, respectively, [37,38]. Size distributions were measured for different focusing fluxes to check the cluster breakup. Aggregated samples of initial monodisperse latex of 747 ± 67 nm radius (Rhône-Poulenc, batch: K 080/889) were analyzed. We chose this monomer size because the cluster breakup appears earlier as the monomer size increases. Discrepancies in the distributions never exceeded 10%. This difference is explained by taking into account the statistical error ($N_i^{1/2}$) and the extra dust appearing for larger focusing fluxes, which may be corrected by subtracting the size distribution measured, with supernatant only. From these results we conclude that the cluster breakup does not affect our experiments since they were carried out using smaller monomers.

C. Experimental system

The experimental system was a conventional polystyrene latex (Sekisui-N1A19E) with a negative surface charge due to the sulphate groups. The radius of the spherical microspheres, 292 ± 19 nm, was determined by the transmission electron microscopy. The latex particles were cleaned by

TABLE I. Electrophoretic mobility, electrokinetic surface charge density, and the stability of the colloidal particles for the three experimental cases.

Experimental case	pH	$-\mu_e/10^{-8}$ ($m^2\,V^{-1}\,s^{-1}$)	$-\sigma_{ek}/10^{-2}$ (C/m^2)	c.c.c (M)	W
I	2.3±0.1	0.2±0.1	0.1±0.1	≈0.00	1.9±0.2
II	4.2±0.1	2.1±0.2	0.8±0.2	≈0.10	1.9±0.2
III	9.3±0.1	3.7±0.2	1.5±0.2	≈0.35	3.2±0.4

centrifugation and then by the ion exchange over a mixed bed. Buffers were used to set the pH of the samples: acetate at pH 4 and borate at pH 9. All chemicals used were of A. R. quality and twice-distilled water was purified using Millipore equipment. The critical coagulation concentration (c.c.c.) was determined directly by dilution of the latex particles in the solutions of the different salt concentration. The electrophoretic mobility of the particles μ_e, was measured using a Zeta-Sizer IIc device (Malvern Instruments, U.K.) to control the modification in the charge produced by the pH. μ_e was determined as a function of the pH at 0.015 M of the ionic concentration. In every case it was found that $\mu_e<0$, which confirmed the negative sign of the surface charge. Mobility was converted into ζ potential using Smoluchowski's theory [39,40]. The electrokinetic surface charge $\sigma_{\rm ek}$ was calculated using the Gouy-Chapman model for the electric double layer (e.d.l.) [39]. Table I shows the three experimental cases studied. In case I, the system is practically at its isoelectric point and therefore $\sigma_{\rm ek}\approx 0$. In case II, the electrokinetic charge is larger by an order of magnitude than in the previous case, and in case III the charge is larger by a further factor of 2. Table I also shows the critical KCl concentration of the suspensions at different pH. In part IV of this article, the stability of the system at different pH is discussed from the data obtained by monitoring the kinetics using the single particle instrument.

D. Experiment details

Prior to undertaking our studies, fresh suspensions of microspheres were sonicated for 30 mins to breakup any initial clusters. Aggregation was initiated by mixing the microspheres suspended in the salt-free water and the aggregation agent. Aggregations were induced at high ionic concentration; 0.5 M of KCl, higher than the c.c.c.. Immediately afterwards, the timer was started.

The aggregation experiments were carried out in a reaction vessel at 20±1 °C and an initial particle concentration of $N_0=4.0\times10^8$ cm^{-3}. The cluster sedimentation due to the slight difference between the polystyrene and the water densities was negligible. Precautions were taken so that nondestructive size distribution analysis could be performed. Small portions of the aggregating colloid were slowly taken from the suspensions through a wide aperture pipette. Samples were diluted in the same solvent used for the dispersions in order to stop the aggregation during the measurements. No variations of the cluster-size distribution were detected while the samples were kept in the dilute medium for several hours. Moreover, the particle concentration was optimized to ensure a single particle detection ($\approx10^7$ cm^{-3}). Cluster size distribution was monitored and histograms were taken at the different aggregation steps. These measurements allowed the cluster size distribution to be determined.

IV. RESULTS AND DISCUSSION

A. Stability

In order to determine the regime of the aggregation processes, the experimental rates of aggregation were determined for each experimental case and compared with the theoretical prediction for the diffusion aggregation. To ensure the DLCA regime, the rate of aggregation must match the prediction set by diffusion. From the initial time dependence of the cluster-size distributions, the experimental Smoluchowski rate constants were determined using Eq. (4). For cases I and II, $k_s=\frac{1}{2}k_{11}=(2.8\pm0.3)\times10^{-12}$ $cm^{-3}\,s^{-1}$. This value falls within the range of values commonly reported for fast aggregation [17,33,37,41–50]. For case III the rate constant is $k_s=(1.7\pm0.3)\times10^{-12}$ $cm^{-3}\,s^{-1}$, lower than in the previous cases. The theoretical Smoluchowski rate constant for a system of identical spherical particles is [12] $k_s^{\rm brow}=4/3\ K_BT/\eta=5.5\times10^{-12}$ $cm^{-3}\,s^{-1}$, from our experimental conditions. Table I shows the stability factor, $W=k_s^{\rm brow}/k_s^{\rm exp}$, for the different experimental cases.

In order to explain the lower value of the experimental reaction constant with respect to the theoretical one, viscous interaction between the particles was considered [40,51,52]. The Brownian diffusivity for relative motion, $D_{12}=K_BT/f$ (f is the hydrodynamic resistance coefficient), was numerically assessed using formulas in the Spielman article [52]. The theoretical Smoluchowski rate constant was calculated; $k_s^{\rm vis}=k_s^{\rm brow}/1.97=2.8\times10^{-12}$ $cm^{-3}\,s^{-1}$, which agrees with the experimental one, for cases I and II.

For cases I and II, the DLCA conditions are satisfied. For case III, the stability factor is higher than in the previous cases. This is due to the repulsive forces appearing when the surface charge of the particles increases. Thus, in case III, the DLCA conditions are not completely achieved.

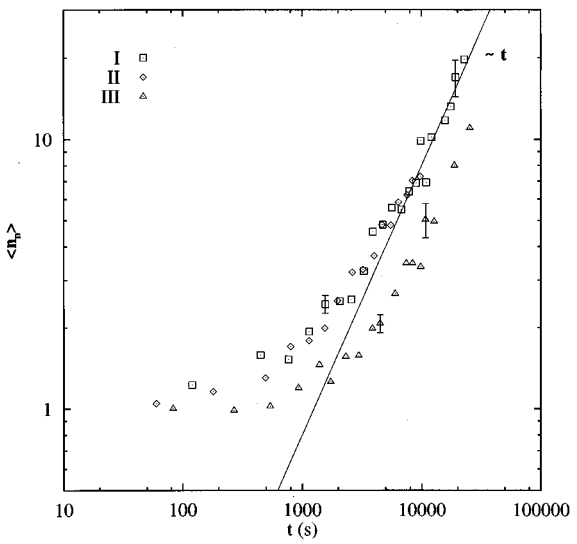

FIG. 3. Time evolution of the number-average mean cluster size for cases I, II, and III. In every case, the mean cluster size grows linearly at long times. In case III the growth is slower than in cases I and II, which agrees with the stability measurements.

B. Dynamic scaling

We now analyze our data using the dynamic scaling formalism. The main questions are: whether or not the cluster-size distributions scale; when the scaling becomes apparent; and what mechanism governs the aggregation. For this purpose, the number-average mean cluster size $\langle n_n \rangle = N_0/M_0(t)$ was determined by measuring the zero moment of the size distribution, $M_0 = \Sigma N_n$. This is related to $s(t)$ and, together with the distribution $N_n(t)$, allows the scaling function $\Phi(x)$ to be determined.

Function $s(t)$. Figure 3 shows the time dependence of $\langle n_n \rangle$. For cases I, II, and III, $\langle n_n \rangle \sim t$ was found at long times. In case III, the kinetics is slower than in cases I and II, which agrees with the higher stability of the system.

The relationship between $\langle n_n \rangle$ and the scaling function $s(t)$ depends on the sign of μ (9). In order to determine this sign we plotted N_n vs n (Figs. 4), observing that in cases I and II [4(a) and 4(b)], it reaches peaks when the aggregation time increases. This suggests $\mu < 0$ (12) and thus, the relationship $s(t) \sim \langle n_n \rangle$ is satisfied. Depletion of the small clusters is a characteristic of the DLCA.

Nevertheless, in case III [Fig. 4(c)], the distribution develops a power-law decay in n at long times, given by $N_n \sim n^{-1}$, which suggest $\mu \geqslant 0$ (12). Power-law decay is a characteristic of the RLCA [53]. In order to determine whether μ is greater than or equal to zero, the long time dependence of the cluster-size distribution was determined to be $N_n(t) \sim t^{-(0.8 \pm 0.1)}$. For kernels with $\mu = 0$ theory predicts $N_n(t) \sim t^{-w}$ with $w > 1$ (12). Thus, the exponent $-(0.8 \pm 0.1)$,

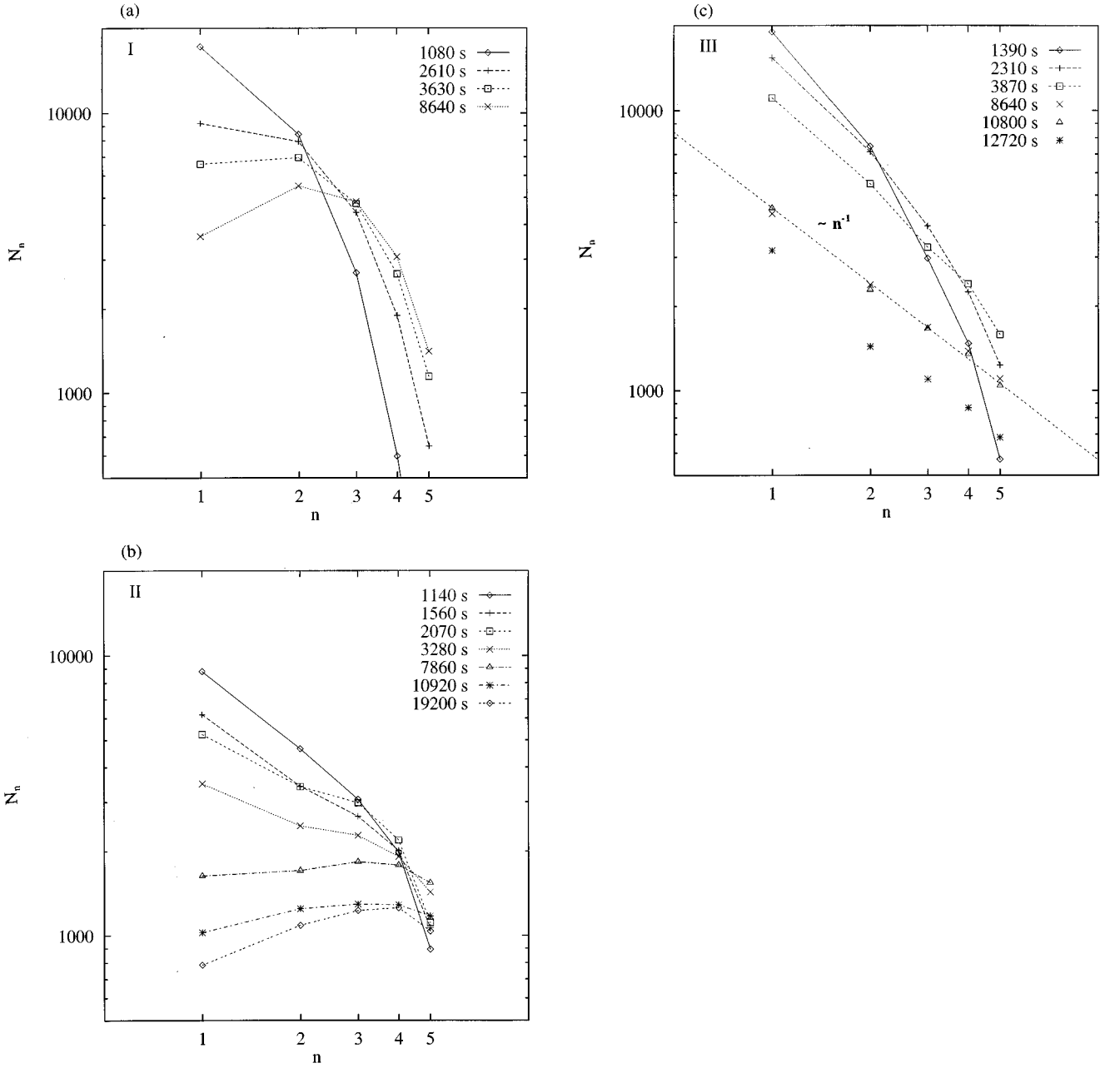

FIG. 4. Plots of $N_n(t)$ versus n for different times. In cases I and II, a peak is developed at a long times, which indicates $\mu < 0$. For case III, a power-law decay is shown, which suggests that $\mu \geqslant 0$. The error in N_n is assumed to be proportional to $N_n^{1/2}$.

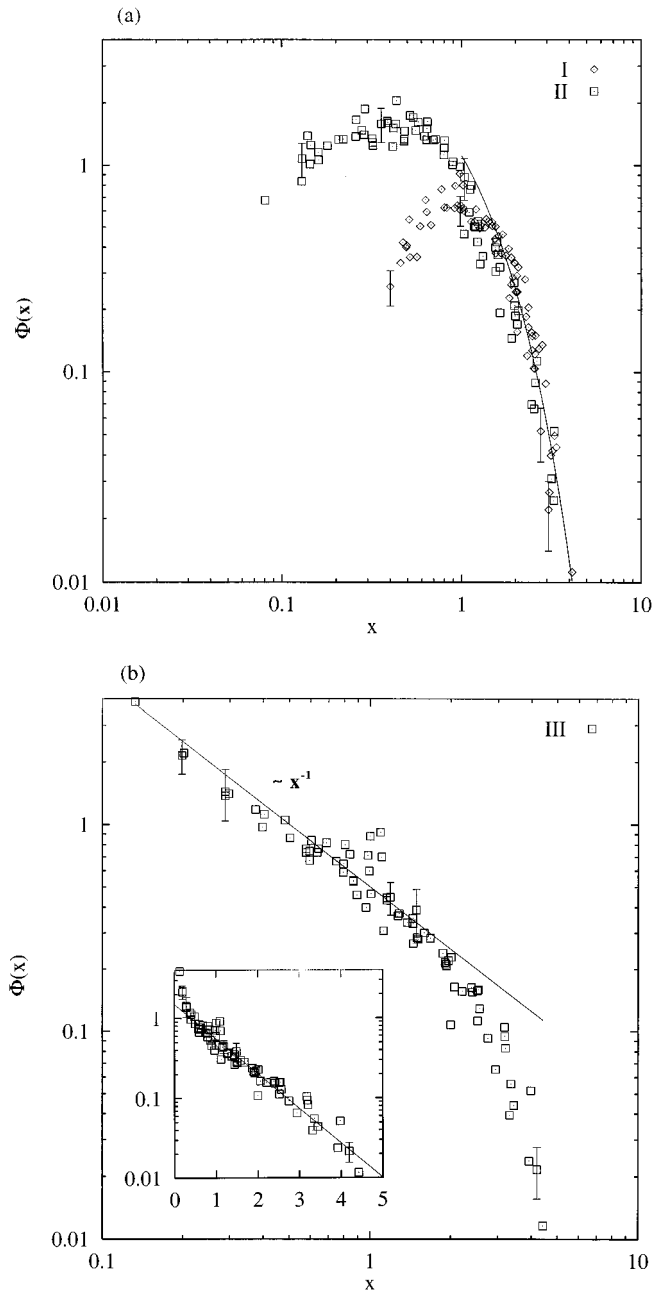

FIG. 5. Experimental $\Phi(x)$ distributions. The distributions are aligned for different times, showing dynamic scaling. For cases I and II, bell-shaped curves confirm the negative sign of μ. A shift in the maximum position is observed when the surface charge rises. For case III $\Phi(x)$ decays monotonically, demonstrating that the sign of μ has changed to $\mu \geqslant 0$. For $x>1$, a decreasing exponential behavior is shown in every case (solid lines), which suggests $\lambda \approx 0$.

close to one, suggests that $\mu>0$. For kernels with $\mu>0$, the coagulation equation also predicts $N_n \sim n^{-(1+\lambda)}$ (12) and thus, from the experimental exponent of n we find $\lambda \approx 0$. Consequently, the relationship $s(t) \sim \langle n_n \rangle$ is also satisfied for case III when the value $\lambda=0$ is used in Eq. (9).

Therefore, for every case, $s(t)$ shall be identified with $\langle n_n \rangle$, and thus, the relationship $\langle n_n \rangle \sim t^{1/(1-\lambda)}$, when $\lambda=0$ (8), reproduces the experimental results, shown in Fig. 3.

Time-independent scaling distribution $\Phi(x)$. $\Phi(x)$ was determined by plotting $s^2(t)N_n(t)/N_0$ versus $x \equiv n/s(t)$ for different times. For aggregation times longer than the characteristic aggregation time, $t_{agg} \equiv 2/N_0 k_s^{exp}$, the data collapses along a single master curve (Figs. 5). These results demonstrate that the scaling approach is appropriate for the experimental data. It is really surprising since the data corresponding to $t \approx t_{agg}$ does not represent the scaling limes; large clusters and long times. This was also observed by Broide and Cohen [8]. Figure 5(a) plots this function up to $t \approx 21\ t_{agg}$ and $t \approx 12\ t_{agg}$ for cases I and II, respectively. Figure 5(b) shows $\Phi(x)$ for case III up to $t \approx 14\ t_{agg}$.

In cases I and II bell-shaped curves appear, which confirms the negative sign of μ (11). Furthermore, a shift in the maximum position is observed. From our measurements we can obtain information about the sign of μ but not its exact value. Nevertheless, it is interesting to comment that the shift in the maximum position agrees with the theoretical prediction if we accept $|\mu| \approx 0$, where kernels with $\mu<0$ show typical $\mu=0$ behavior for x in the intermediate range, $x_0 \ll x \ll 1$. Therefore, the shift in x_0 would be qualitatively interpreted as a change of μ towards zero when the surface charge density increases (see theory).

The stability factor W was found by monitoring the evolution of the cluster-size distribution for short times. Furthermore, the scaling behavior is exhibited for longer times. Cases I and II both have the same W and yet they have different scaled distributions. This raises an important question: Does W uniquely determine the scaled distribution? Given our experimental results the answer is negative. There is not enough information during the first stages of the aggregation to predict the entire evolution of the system.

In case III, $\Phi(x)$ decays monotonically for every x, which confirms that $\mu \geqslant 0$ (11), and from the time dependence of the cluster-size distribution, we conclude that $\mu>0$. Figure 5(b) shows that $\Phi(x<1) \sim x^{-1}$. For kernels with $\mu>0$, the theory predicts, $\Phi(x \ll 1) \sim x^{-(1+\lambda)}$ (11). Thus, our result leads to $\lambda \approx 0$, which confirms the value directly obtained from the cluster-size distribution [Fig. 4(c)].

A decreasing exponential behavior for $x>1$ was found for cases I, II and III. Theory predicts for $x \gg 1$ a μ independent behavior given by (10). Several values of λ were tried, concluding that the best fitting leads to $\lambda \approx 0$, which is in line with the value obtained above. Experimental uncertainty in $\Phi(x)$ does not allow the value of λ to be found accurately.

To sum up, our results indicate that in all the processes, induced at high salt concentrations, the homogeneity parameter has a value of zero. This result is in line with the DLCA experiments [5,7,8,23,24,54–58]. However, in the absence of a surface charge (case I), the exponent μ is negative. This result is also in line with the DLCA experiments [23,33]. The exponent μ could drift towards zero as the charge is increased (case II) and finally, changes its sign when the charge increases even more (case III). The positive sign of μ is in line with the measurements of the slow aggregation [8]. Table II shows the stability data and the kinetics characteristic for every case.

The original Smoluchowski kernel [12], developed to describe the DLCA, gives the reaction rate as a collision cross section due to the diffusion of spheres in radius R, having a diffusion constant $D=K_B T/6\pi\eta R$. This kernel with $\lambda=0$ and negative μ, can be used for describing our experimental results in cases I and II. A more realistic description is made

TABLE II. Summary of the stability data and the long time kinetics.

Experimental case	W	$\langle n_n \rangle(t)$	$N_n(t)$	$\Phi(x)$	λ	μ	Regime
I	1.9 ± 0.2	$\sim t$	peaks	peaks	0	<0	DLCA
II	1.9 ± 0.2	$\sim t$	peaks	peaks	0	<0	DLCA
III	3.2 ± 0.4	$\sim t$	decays	decays	0	>0	Intermediate

when clusters are considered as fractal structures. Thus, the relationship between the gyration radius of an i-mer and the radius of a monomer is expressed as $R_i = R_0 i^{1/d_f}$. For the diffusion constant $D_i = (K_B T/6\pi\eta R_0) i^{-1/d_f}$ [59]. d_f and d_h are the fractal and hydrodynamic fractal dimension, respectively. The Brownian kernel is, thereby

$$k_{ij} = \frac{2K_B T}{3\eta} (i^{1/d_f} + j^{1/d_f})(i^{-1/d_h} + j^{-1/d_h}). \tag{13}$$

Thus, the aggregation exponents are $\lambda = 1/d_f - 1/d_h$ and $\mu = -1/d_h$. In our experiments, we found $\lambda \approx 0$ and therefore $d_f \approx d_h$, which is reported by direct measurements of d_f and d_h [60,61] and by computer simulations [59]. This kernel also predicts a negative value of μ, in agreement with our experimental results. Recently, Thorn and Seesselberg [62] have used a stochastic simulation method to recover the scaling behavior of the microsphere colloids. They simulate processes using the Brownian kernel with the monodisperse initial conditions. The value $d_f = 1.75$ and $d_f \approx d_h$ were accepted for the DLCA simulation. They found a bell-shaped $\Phi(x)$ curve which agrees with our experimental results.

In case III, μ is positive and the Brownian kernel fails to fit the experimental results. The positive sign of μ is interpreted by a greater reactivity between the larger-sized clusters when the surface charge density increases. The power-law decay in the cluster-size distributions ($\mu \geq 0$) [Figs. 4(c) and 5(b)], the asymptotic time dependence ($\mu > 0$) and the stability data suggest that in case III the process is not DLCA. On the other hand, the value of λ, close to zero, that we have found does not indicate slow aggregation, and it is far from the exponent $\lambda = 1$ predicted analytically for the RLCA kernels [53]. For slow aggregation the values $\lambda \approx \frac{1}{2}$ [7,33,63,64] and $\lambda \approx 1$ [5,54–56,65] were found by other authors. For example, Asnaghi *et al.* and Olivier and Sorensen studied the colloidal aggregation in the intermediate regimes, finding that λ changes continuously from 0 to 0.5 when they change the aggregation conditions from fast to slow aggregation. Probably, in case III, we observe an intermediate regime between DLCA and RLCA. The stability data and the kinetics of the process indicate that in case III the residual interaction between particles controls the aggregation mechanism. Thorn and Seesselberg [62] also studied the scaling behavior under slow aggregation conditions, finding $\mu \geq 0$ and $\lambda \approx \frac{1}{2}$. An interesting question for future research would be to simulate the aggregation of these kinds of systems, including a residual interaction between particles.

V. CONCLUSIONS

The temporal evolution of the cluster-size distributions has been measured using a single particle light scattering instrument. Measurements were carried out at a high salt concentration and different surface charge densities. In all cases, we found that distributions exhibit dynamic scaling for times longer than t_{agg}.

For particles with low surface charge density, the scaled size distribution is bell shaped, with a shift appearing at the maximum position when the charge is increased. In this case, the kernel is characterized by the parameters $\lambda \approx 0$ and $\mu < 0$, which agrees with the value of the exponents for the Brownian kernel and with results obtained by the simulation using this kernel. Thus, for the low surface charge densities, our results are in accord with the DLCA. Big clusters bind preferentially to small clusters. The shift in the position of the maximum might be due to a change in the value of the parameter μ towards zero. Moreover, for the low surface charge densities, the same value for W does not guarantee the same scaled distribution.

When the particle surface charge density increases even more, we find that the distribution exhibits a power-law decay, which demonstrates that the aggregation mechanism changes. In this case we found $\lambda \approx 0$ and $\mu > 0$. Thus, for the highest particle's surface charge density, the residual interaction controls the aggregation, and when this interaction increases, big clusters bind preferentially to big clusters. This result suggests that the residual electrostatic interaction could control the reactivity between big and small clusters.

ACKNOWLEDGMENTS

We thank M. Cohen Stuart for helpful discussions when the single particle detection instrument was constructed. We also acknowledge with thanks the constructive and clarifying discussions with J. E. Martin. This work was supported by CICYT (Spain), Project MAT 94-0560.

[1] *Kinetics of Aggregation and Gelation*, edited by F. Family and D. P. Landau (North-Holland, Amsterdam, 1984).
[2] D. H. Sutherland, J. Colloid Interface Sci. **25**, 373 (1967).
[3] G. K. von Schulthess and G. B. Benedek, Macromolecules **13**, 939 (1980).
[4] J. E. Martin, J. P. Wilcoxon, D. Schaefer, and J. Odinek, Phys. Rev. A **41**, 4379 (1990).
[5] G. Bolle, C. Cametti, P. Codasefano, and P. Tartaglia, Phys. Rev. A **35**, 837 (1987).
[6] H. Y. Lin, H. M. Lindsay, D. A. Weitz, R. C. Ball, R. Klein, and P. Meakin, Phys. Rev. A **41**, 2005 (1990).
[7] D. Asnaghi, M. Carpineti, M. Giglio, and M. Sozzi, Phys. Rev. A **45**, 1018 (1992).
[8] M. L. Broide and R. J. Cohen, Phys. Rev. Lett. **64**, 2026 (1990).
[9] M. Carpineti and M. Giglio, Adv. Colloid Interface Sci. **46**, 73 (1993).
[10] J. Stankiewicz, M. Cabrerizo-Vílchez, and R. Hidalgo-

Álvarez, Phys. Rev. E **47**, 2663 (1993).
[11] R. Jullien, Comments Cond. Mat. Phys. **13**, 177 (1987).
[12] M. Von Smoluchowski, Z. Phys. Chem. (Leipzig) **92**, 129 (1917).
[13] T. Vicsek, *Fractal Growth Phenomena* (Word Scientific, Singapore, 1992).
[14] B. B. Mandelbrot, *The Fractal Geometry of Nature* (Freeman, New York, 1982).
[15] J. Cahill, P. G. Cummins, E. J. Staples, and L. G. Thompson, J. Colloid Interface Sci. **117**, 406 (1987).
[16] P. McFadyen and A. L. Smith, J. Colloid Interface Sci. **45**, 573 (1973).
[17] E. G. M. Pelssers, M. C. A. Stuart, and G. J. Fleer, J. Colloid Interface Sci. **137**, 350 (1990); **137**, 362 (1990).
[18] D. J. Walsh, J. Anderson, A. Parker, and M. J. Dix, Colloid Polym. Sci. **259**, 1003 (1981).
[19] N. Buske, H. Gedan, H. Lichtenfeld, W. Katz, and H. Sonntag, Colloid Polym. Sci. **258**, 1303 (1980).
[20] G. L. Beyer, J. Colloid Interface Sci. **118**, 137 (1987).
[21] M. S. Bowen, M. L. Broide, and R. J. Cohen, J. Colloid Interface Sci. **105**, 605 (1985); **105**, 617 (1985).
[22] M. Bartholdi, G. C. Salzman, R. D. Hielbert, and M. Kerker, Appl. Opt. **19**, 1573 (1980).
[23] E. Pefferkorn and R. Varoqui, J. Chem. Phys. **91**, 5679 (1989).
[24] D. A. Weitz and M. Y. Lin, Phys. Rev. Lett. **57**, 2037 (1986).
[25] T. Vicsek and F. Family, Phys. Rev. Lett. **52**, 1669 (1984).
[26] P. G. J. Van Dongen and M. H. Ernst, Phys. Rev. Lett. **54**, 1396 (1985).
[27] R. M. Ziff, *Kinetics of Aggregation and Gelation*, edited by F. Family and D. P. Landau (North-Holland, Amsterdam, 1984).
[28] F. Leyvraz and H. R. Tschudi, J. Phys. A **15**, 1951 (1982).
[29] R. M. Ziff, M. H. Ernst, and E. M. Hendriks, J. Phys. A **16**, 2293 (1983).
[30] E. M. Hendriks, M. H. Ernst, and R. M. Ziff, J. Stat. Phys. **31**, 519 (1983).
[31] A. A. Lishnikov, J. Colloid Interface Sci. **45**, 549 (1973).
[32] M. H. Ernst, in *Fractals in Physics*, edited by L. Pietronero and E. Tosatti (North-Holland, Amsterdam, 1986).
[33] M. L. Broide and R. J. Cohen, J. Colloid Interface Sci. **153**, 493 (1992).
[34] T. W. Taylor and C. M. Sorensen, Phys. Rev. A **36**, 5415 (1987).
[35] A. Fernández-Barbero, Ph.D. thesis, Universidad de Granada, 1994.
[36] M. Kerker, *The Scattering of Light and Other Electromagnetic Radiations* (Academic, New York, 1969).
[37] J. Cahill, P. G. Cummins, E. J. Staples, and L. G. Thompson, J. Colloid Interface Sci. **117**, 406 (1987).
[38] L. Goren, J. Colloid Interface Sci. **36**, 94 (1971).
[39] See for example, R. Hidalgo-Álvarez, Adv. Colloid Interface Sci. **34**, 217 (1992).
[40] A. Fernández-Barbero, A. Martín-Rodríguez, J. Callejas-Fernández, and R. Hidalgo-Álvarez, J. Colloid Interface Sci. **162**, 257 (1994).
[41] J. Cahill, P. G. Cummins, E. J. Staples, and L. G. Thompson, Colloids Surf. **18**, 189 (1989).
[42] H. Gedan, H. Lichtenfeld, H. Sonntag, and H. J. Krug, Colloids Surf. **11**, 199 (1984).
[43] W. I. Higuchi, R. Okada, G. A. Sterter, and A. P. Lenberger, J. Pharm. Sci. **52**, 49 (1963).
[44] B. A. Mathews and C. T. Rhodes, J. Pharm. Sci. **57**, 557 (1969).
[45] A. Lips and E. J. Willis, J. Chem. Soc. Faraday Trans. **69**, 1226 (1973).
[46] W. Hatton, P. McFadyen, and A. L. Smith, J. Chem. Soc. Faraday Trans. **70**, 665 (1974).
[47] J. W. Lichtenfelt, C. Pathmanoharan, and P. H. Wiersema, J. Colloid Interface Sci. **49**, 281 (1974).
[48] M. L. Broide, R. J. Cohen, J. Colloid Interface Sci. **105**, 605 (1985); **105**, 617 (1985).
[49] K. Higashitanti, M. Kondo, and A. Matacle, J. Colloid Interface Sci. **142**, 204 (1991).
[50] A. Fernández-Barbero, A. Schmitt, M. Cabrerizo-Vílchez, and R. Martínez-García, Physica A (to be published).
[51] E. P. Honig, G. J. Roebersen, and P. H. Wiersema, J. Colloid Interface Sci. **36**, 97 (1971).
[52] L. A. Spielman, J. Colloid Interface Sci. **33**, 562 (1970).
[53] R. C. Ball, D. A. Weitz, T. A. Witten, and F. Leyvraz, Phys. Rev. Lett. **58**, 274 (1987).
[54] C. Aubert and D. S. Cannel, Phys. Rev. Lett. **56**, 738 (1986).
[55] H. Y. Lin, H. M. Lindsay, D. A. Weitz, R. C. Ball, R. Klein, and P. Meakin, Nature (London) **339**, 360 (1989).
[56] Z. Zhou and B. Chu, J. Colloid Interface Sci. **143**, 356 (1991).
[57] M. Carpineti, F. Ferri, M. Giglio, E. Paganini, and U. Perini, Phys. Rev. A **42**, 7347 (1990).
[58] H. Y. Lin, H. M. Lindsay, D. A. Weitz, R. Klein, R. C. Ball, and P. Meakin, J. Phys. Condens. Matter **2**, 3093 (1990).
[59] P. Meakin, Z. Chen, and J. M. Deutch, J. Chem. Phys. **82**, 3786 (1985).
[60] P. Wiltzius, Phys. Rev. Lett. **58**, 710 (1987).
[61] P. N. Pusey and J. G. Rarity, Molec. Phys. **62**, 411 (1987).
[62] M. Thorn and M. Seesselberg, Phys. Rev. Lett. **72**, 3662 (1994).
[63] J. P. Wilcoxon, J. E. Martin, and D. W. Shaefer, Phys. Rev. A **39**, 2675 (1989).
[64] B. J. Olivier and C. J. Sorensen, J. Colloid Interface Sci. **134**, 139 (1990).
[65] J. E. Martin, Phys. Rev. A **36**, 3415 (1987).